Journal of Materials Chemistry A

Accepted Manuscript

ROYAL SOCIETY OF CHEMISTRY

www.rsc.org/materialsA

Journal Name

ARTICLE

Nickel-decorated graphene nanoplates for enhanced H_2 sorption properties of magnesium hydride at moderate temperatures

Received 00th January 20xx,
Accepted 00th January 20xx

DOI: 10.1039/x0xx00000x

www.rsc.org/

Jiguang Zhang, Yunfeng Zhu,* Xiaoxian Zang, Qingqing Huan, Wei Su, Delong Zhu and Liquan Li

Magnesium hydride is considered as an ideal candidate for effective hydrogen storage due to its high gravimetric hydrogen capacity and accessibility. But its use as a commercial material is hindered by its relatively high operating temperatures and slow release/uptake kinetics. To solve this, we first synthesize Ni decorated graphene nanoplates (Ni/Gn) catalysts with high dispersed metal nano particles (NPs) via a facile method, then the as-prepared Ni/Gn catalysts were introduced by using the hydriding combustion synthesis and mechanical milling (HCS+MM) method to obtain Mg-based composites. Remarkable enhancement of hydrogen sorption rates have been found for these composites in the presence of Ni/Gn additives, especially for the $Mg@Ni_8Gn_2$ sample: hydrogen absorption amount of 6.28 wt.% within 100 s at 373 K and hydrogen desorption amount of 5.73 wt.% within 1800 s at 523 K. A rather low activation energy (71.8 kJ/mol) for the dehydrogenation of MgH_2 was determined in the same sample, allowing that the relatively moderate temperatures are required to absorb/desorb hydrogen. The excellent hydrogen sorption rates for the composites are thought to be associated with the high dispersity of in situ formed nanometric Mg_2NiH_4 particles during the HCS+MM process. In addition, a microstrain-induced synergetic hydrogen sorption mechanism is proposed, being correlated by the local introduction of Mg_2Ni nano catalyst into the Mg matrix.

Introduction

The global economic growth today is obtained at the expense of the huge consumption of traditional fossil fuel resources (coal, oil and gas) and the ecological crisis, threatening the sustainable development of our society. Besides maximizing the efficiency of the existing energy, it is crucial to exploit clean alternative energy carriers, especially those renewable ones, which are meant to gradually reduce our reliance on carbon-based fossil fuels. [1] Among those potential candidates, hydrogen, carbon-free and non-toxic, is very prospective and has been the focus of attention over the last several decades. Scientists claim that the 21st century will be the era of hydrogen energy, which may surely become one of the most important energy media in the future society.[2,3] For its widespread utilization, especially the mobile application of hydrogen, a lot of issues are still await to be solved, including the invention of safe hydrogen storage materials with high-efficiency,[4] the large-scale hydrogen production, safe transportation and the controllable combustion of hydrogen.

An increasing amount of attention has been paid to the exploration of approaches, by which sufficient hydrogen with desirable kinetics can be stored at relatively moderate operating conditions. In the solid state hydrogen storage medium systems, metal hydrides have been intensively studied due to the safe and high hydrogen content in terms of both gravimetric and volumetric densities.[5-8] As a very representative light metal, magnesium seems to be an appropriate choice to be used as a hydrogen store owing to its high gravimetric (7.6 wt.%) and volumetric capacity (110 g/L), low cost, natural abundance and environmental friendliness. Continuous researches on magnesium hydride have been carried out despite its intrinsic drawbacks, i.e., undesirable thermodynamic properties and sluggish absorption/desorption kinetics, deriving from its high desorption enthalpy and slow hydrogen diffusion rate inside Mg or MgH_2 bulk.[9-11]

Plenty of methods newly discovered have been proved to be helpful for the design and synthesis of magnesium hydride system, covering both physical and chemical means and considerable progress has thus been made.[12-18] It should be emphasized that, although innovative, those methods are still generally designed in accordance with the following four basic strategies for the improvement of comprehensive hydrogen sorption properties.

1) Nanosizing The existing theoretical calculations have already foreseen the nanometer effects of magnesium hydride. It is suggested that magnesium hydride would destabilize significantly with a sharp reduction in the desorption temperature when the crystal grain size becomes smaller than 2

College of Materials Science and Engineering, Nanjing Tech University, 5 Xinmofan Road, Nanjing, 210009, P.R. China. E-mail: yfzhu@njtech.edu.cn

† Electronic Supplementary Information (ESI) available: [Fig. S1~S5]. See DOI: 10.1039/x0xx00000x

nm, and at the same time, the desorption kinetics can be greatly improved, because of the abundant and short hydrogen diffusion path owing to the grain refinement.[19-22] However, it is rather difficult to experimentally obtain magnesium hydride particles with only a few nanometers. More recently, many groups attempt to load nano-MgH_2 into/onto various scaffolds, such as carbon aerogel and mesoporous carbon, forming a hybrid MgH_2-carbon nanoconfined system.[23-29]

2) Alloying with other elements Mg-based alloys (e.g., Mg_2Ni) have been proved to display better thermal instability of the hydrides than the pure magnesium. Alloying Mg with suitable transition metal elements leads to crystal lattice transformation and affects to some extent the thermodynamic and sorption kinetics of the materials.[30-33] The drawback of this alloying route is, in all cases, the inevitable reducing of the reversible hydrogen storage capacity. To handle this, a favorable solution is to prepare MgH_2-rich complex hydrides, i.e., MgH_2-Mg_2NiH_4 composite, providing a substantial decrease in hydride stability without significant loss of the hydrogen storage capacity.[32, 34]

3) Surface modification High active surface with large area of the active substance is crucial to the sorption reaction. On the other hand, however, magnesium nanoparticles will become non-stabilized and thus suffer from oxidation and passivation, which seriously hinder the hydrogen diffusion during hydrogen sorption process. This is actually a dilemma. One should keep balance between providing enough active sites for hydrogenation/dehydrogenation reaction and protecting the particle surface from oxidizing.[17, 35, 36]

4) Introduction of catalysts The catalysts play an extraordinarily important role in accelerating the sorption rate and even destabilizing the Mg-H bonding energy in the metal-catalyzed magnesium hydride system. The additional catalysts are generally supposed to act as activation agents so as to form intermediate metastable states, facilitating reaction rate as a whole. To achieve this, various additives have been introduced to the Mg hydride system.[37-42] Scaffolds materials with large specific surface area like carbon-based materials and MOFs are often introduced as a substrate for the metal catalysts particles,[43, 44] providing space confinement or dispersive effect whereby enhancing their catalytic ability as to hydrogen sorption kinetics of Mg/MgH_2.

Our recent publication concerning carbon-based catalysts associated with Mg-based hydrides focused on the roles of metal-assisted multi-wall carbon nanotubes (MWCNTs) hybrids, in which an extraordinarily synergetic catalytic effect between MWCNTs and supporting metallic particles is revealed.[45] Alternatively, in the carbon family, graphene, a bidimensional monolayer sp2 carbon atom arranged in a hexagonal network, is known as the mother of all graphic materials. What makes graphene and graphene-based materials unprecedentedly attractive, especially in the energy-related catalytical areas, are not only their superior electronic and mechanical properties in comparison with the other carbon allotropes, but also the unique 2-D nanostructure with high chemical stability, which makes it an ideal host to sufficiently disperse NPs through a space confinement effect or a pinning effect via suitable synthesized method.[46]

In this context, we report a fantastic combination of Mg-based hydrides and graphene nanoplates (Gn) with remarkable sorption properties at moderate temperatures. To achieve this, a series of novel nanohybrids, namely, functional graphene nanoplate supported nickel additives were initially synthesized using chemical routes. Then they were introduced into the HCS procedure at a 2.0 MPa hydrogen atmosphere to form Mg-based hydrides composite materials, which were subsequently treated by a short-time mechanical milling. It was found that the introduction of Ni/Gn dramatically enhanced the sorption properties of the composites by in-situ forming nanosized Mg_2NiH_4 catalytic phase. The $Mg@Ni_8Gn_2$ sample absorbed as high as 6.28 wt.% of hydrogen within 100 s at 373 K and desorbed 5.37 wt.% of hydrogen within 1800 s at 523 K. Detailed hydrogen sorption properties for the samples with Ni/Gn additives of different Ni loading contents at relatively moderate temperatures were presented. Their kinetics and thermodynamics of hydrogen sorption as well as possible explanations were discussed. To our knowledge, this is the first reported work on the prominent hydrogen sorption performance in the presence of metal-assisted graphene catalysts, which indicates a feasible route for the hydrogen storage property enhancement under mild conditions of the light weight metal hydrides and thus offers possibilities of the future mobile applications.

Experimental details

Chemicals

Analytical reagent (AR) grade graphene nanoplates (0.5-10 μm in diameter and 20-50 nm thick, see Fig. S1, ESI†) were purchased from XFNANO Material Technologic Co. Ltd. (Nanjing, China). Original powders of Mg (99.7 wt.% in purity and <100 μm in size), Ni (99.7 wt.% in purity and <50 nm in size), $Ni(NO_3)_2{\cdot}6H_2O$ (AR, 99.7 wt.% in purity), concentrated nitric acid (65 wt.% in purity) and acetone (AR, 99.5 wt.% in purity) were commercially gotten.

Preparation of Ni/Gn nano hybrid catalysts

Graphene nanoplates were originally treated in concentrated nitric acid to ensure functionalization by introducing i.e., carboxylic, carbonyl and hydroxyl groups on their surfaces, which may provide nucleation sites for subsequent deposition of metal species.

A method of direct chemical synthesis was used to synthesize Ni decorated graphene nano hybrids. Typically, graphene nanoplates and $Ni(NO_3)_2{\cdot}6H_2O$ with set mass ratios of Ni:Gn (2:8, 4:6, 6:4 and 8:2) were dispersed into 50 ml acetone by ultrasonic vibration for 1h, before drying in blowing dry oven at 326 K for 8 h. Afterwards, the mixtures were heat-treated at 673 K and held for 4 h in a tube furnace under Ar atmosphere. Finally, they were heated up to 723 K and held for 4 h under H_2 atmosphere to ensure complete reduction of Ni.

Those as-prepared Ni decorated graphene nanoplates hybrids were denoted as Ni_xGn_{10-x} (x=2, 4, 6, 8).

Preparation of $Mg@Ni_xGn_{10-x}$ (x=2, 4, 6, 8) composites

The as-synthesized Ni_xGn_{10-x} (x=2, 4, 6, 8) catalysts and Mg powders mixed in a fixed mass ratio (10: 90) were homogenized by ultrasonic vibration in acetone for 30 min. After being completely dried in air, the powders were directly used for HCS, during which the samples were first heated up to 853 K at a heating rate of 10 K/min under 2 MPa hydrogen atmosphere and then kept at that temperature for 1 h. They were then cooled down to 613 K and held for 2 h until they were cooled down to room temperature. The HCSed products were further mechanical milled for 10 h at a speed of 400 rpm and 40:1 in ball-to-powder ratio in a planetary-type ball mill under argon atmosphere. The final products were denoted as $Mg@Ni_xG_{10-x}$ (x=2, 4, 6, 8). Two comparative samples, Mg@Ni and Mg@Gn with a 90 wt.% of Mg content, were also prepared using the same method to verify the particular effect of the Ni/Gn nano hybrid additives in this study. All of the material handling was carried out in a glove box with O_2 and H_2O concentrations < 1 ppm.

Characterization

The phase compositions and microstructures of the catalysts, along with HCS and HCS+MM products, were examined by means of X-ray diffraction (XRD) with Cu-K_α radiation (40 kV and 35 mA), scanning electron microscopy (SEM, JEOL JSM-6360LV) and high-resolution transmission electron microscope (HRTEM, JEM-2010 UHR). The software Rietica was used for the quantitative phase analysis of the as-synthesized catalysts based on the Rietveld method. The average grain sizes of the main phase MgH_2 in the composites were estimated from the XRD patterns according to Scherrer's equation:

$$D\ \beta\ \cos\theta\ =\ 0.9\ \lambda \qquad (1)$$

Where D is the grain size, λ is the X-ray wavelength of 0.154 nm, β is the full width at half maximum of the diffraction peak and θ is the Bragg angle. Samples of TEM characterization were prepared by ultrasonic shaking of the powder in ethanol and were dried on a copper grid with a holey carbon foil.

The hydrogen storage properties, including thermodynamics and kinetics of the samples, were performed on a Sieverts type pressure-composition-temperature (PCT) volumetric apparatus (GRC, Advanced Materials Co.) at different temperatures. About 0.5 g of the powder for each sample was loaded into a stainless steel sample chamber in the glove box filled with argon. An initial hydrogen pressure of 3.0 MPa and of 0.005 MPa was used for the absorption and desorption kinetics measurements, respectively. Note that since the HCS+MM products were hydrides composites, they suffered from a complete desorption by evacuating upon being heated to 603 K at a heating rate of 10 K/min before the isothermal hydrogen sorption measurements.

Results and discussion

Morphology

Fig.1 shows XRD patterns of as-synthesized Ni_xGn_{10-x} (x=2, 4, 6, 8) samples as well as the raw graphene nanoplates material. The diffraction peaks centering at 2θ≈26.4 and 54.6 degree are brought about by the pristine graphene nanoplates and the rest diffraction peaks at 44.5° (111), 51.7° (200) and 76.4° (220) are attributed to face-centered cubic crystalline nickel (JCPDS data No. 04-0850). There is no evidence for detectable amounts of NiO or $Ni(OH)_2$ phase. According to the Rietveld analysis, the phase abundance of Ni and graphene are calculated to be 61.1 wt.% and 38.9 wt.% for Ni_6Gn_4 sample (Fig. 1b), being very close to the theoretical value. The average crystallite sizes of Ni in Ni_xGn_{10-x} (x=2, 4, 6, 8) additives were calculated to be 25.5 nm, 27.3 nm, 28.5 nm, 35.7 nm, indicating high purity Ni with good crystallinity has been successfully prepared by using this facile chemical method. SEM observations show the uniformly dispersed Ni NPs with an average size of less than 50 nm anchored on the surface of graphene nanoplates for all samples (Fig. 2a-d). Note that for higher Ni loading content, some of the Ni NPs become agglomerated to form wirelike clusters, especially in the case of Ni_6Gn_4 and Ni_8Gn_2 samples (Fig. 2c-d). In addition, even after an intense sonication during the SEM sample preparation, the Ni nanocrystals were still immobilized on the surface of the graphene nanoplates, suggesting a strong interaction between Ni nanoparticles and graphene nanoplates substrate.

The XRD patterns of the HCSed $Mg@Ni_xGn_{10-x}$ (x =2, 4, 6, 8) composites before and after MM are shown in Fig.3. The peaks of the HCS products mainly correspond to β-MgH_2, Mg_2NiH_4, graphite-2H and considerate amount of unreacted Mg (Fig.3 a), which is hard to be avoided in the solid state sintering due to the slow hydriding kinetics of bulk Mg. No detectable amounts of Ni peaks were found, indicating all of the dispersive Ni particles have formed binary intermetallic compound (Mg_2Ni) via an in-situ reaction with Mg during the HCS process. After a short ball milling, as expected, their diffraction peaks become broadening and less pronounced (Fig. 3b), independent of the Ni loading content in the Ni/Gn additives, suggesting the grain refinement of the phases in all the composites. It is supposed that ball milling not only facilitates the formation of a large amount of defects and grain boundaries,[47] but also leads to a good distribution of in situ generated Mg_2Ni hydride, and thus remarkable hydrogen sorption performance could be achieved. Trace of MgO phase was detected owing to the surface oxidation during either the MM process or the sample characterization. The SEM images for the HCS and HCS+MM products of $Mg@Ni_xGn_{10-x}$ (x =2, 4, 6, 8) composites are shown in Fig. S2(see ESI†). The coarse particles of the as-HCSed samples become finer (less than 1μm) and more uniform after the MM treatment. The evidence of graphene nanoplates is hard to be provided partly due to the limited resolution of the SEM in this experiment.

To further characterize the phase structure and distribution of the HCS+MM products, TEM examinations were performed on the HCS+MM $Mg@Ni_8Gn_2$ composite. Fig. 4a exhibits the

bright-field image of a typical aggregate in this composite. Interestingly, after HCS+MM, the graphene nanoplates (evidenced by the inset SAED pattern of region A) could partly keep its sheet-like structure and exhibit an entire distribution in the matrix. As shown in the accompanying SAED pattern of region B (Fig. 4b), the vague continuous diffraction ring-like feature indicates a polycrystalline structure with a high randomness. These diffraction rings are calculated to agree well with the lattice planes of MgH_2 (101), Mg (102) and Mg_2NiH_4 (213), respectively. In order to obtain the dark-field micrograph of the same aggregate, the objective aperture was placed over a portion of the Mg_2NiH_4 (213) diffraction ring. It evidently shows that the in situ formed Mg_2NiH_4 nanoparticles (<20 nm) uniformly disperse in the Mg/MgH_2 matrix and are in good contact with Mg/MgH_2 particles after ball milling modification (Fig. 4c). Very recently, House and his colleagues[48] have investigated the effects of ball milling duration on the microstructure and catalysts' distribution in Ni-catalyzed MgH_2 hydrogen storage materials, by which they demonstrated that the additive catalyst will reside both out of and in the MgH_2 matrix only after a short milling duration, justifying our TEM examinations of the composites. Alternatively, in our work, with high dispersibility and electronic conductivity, carbon-based catalysts Ni_xGn_{10-x} (x =2, 4, 6, 8) were used as the additives and lead to the in situ generation of nano Mg_2NiH_4 particles, which further promote the high dispersion of additional phases in the parent phase matrix. It should be noted that this well-dispersed characteristic of Mg_2NiH_4 particles on the surface or at interfaces of the matrix is detectable throughout the whole sample. The other composites with lower Ni loading amount display similar microstructural characteristics (not shown). A homogenous distribution of catalysts in the matrix is supposed to be crucial to provide a dramatic improvement in terms of the hydrogen sorption properties, especially the kinetic performance of Mg-based hydrides.[49] From the lattice fringes of a typical HRTEM image for the HCS+MM $Mg@Ni_8Gn_2$ composite (Fig. 4d), lattice planes of MgH_2 (101), Mg (102), Mg_2NiH_4 (024) and graphite (002) were identified, as indicated by arrows.

Hydrogen sorption behaviour

Hydrogen absorption/desorption performances of the composites prepared by HCS+MM were conducted in the 373 K—543 K range on a Sieverts type apparatus (GRC, Advanced Materials Co.). The hydrogenation curves at various temperatures under 3.0 MPa are plotted in Fig. 5 and Fig. S3(see ESI†). To evaluate the quick sorption performance of the samples, hydrogen absorption capacities in 100 s are collected and given in Table 1. The hydrogen absorption properties at 373 K (Fig. 5a) is very worthy of noting: due to the absence of metal particles, Mg@Gn sample can hardly be hydrogenated at such a low temperature as a consequence of the sluggish kinetics. However, this could be considerably improved by introducing Ni element. The samples with higher Ni content show faster hydrogen absorption with respect to lower Ni content samples. This is more evident at lower temperatures (see Fig. 5a and Fig. S3a, ESI†). The swiftest absorption kinetics and the amount of hydrogen absorbed as high as 6.28 wt.% are obtained for the $Mg@Ni_8Gn_2$ sample at 373 K, which is 91.8% of its theoretical capacity (7.6×90%=6.84 wt.%). According to our present knowledge, these hydriding results seem to be the best for the samples involving graphene under the same temperature range. Here we highlight the excellent catalytic effect of Ni on the hydrogen absorption kinetics for the Mg hydrides, especially at low temperatures. And this favorable effect of Ni addition will become less outstanding at higher temperatures (Fig. 5b and Fig. S3b-c, ESI†), which is in relation to the susceptibility of sorption kinetics as a function of the temperature of Mg hydrides system. Detailed description about the catalytic effects of Ni addition will be discussed in the following parts.

The hydrogen desorption kinetics for Mg hydride at low temperatures (<473 K) is radically hindered by thermodynamic constrains. As a result, the amount of hydrogen desorbing at these temperatures is practically undetectable for all samples. Fig. S4 (see ESI†) exhibits the hydrogen desorption curves for all the as-synthesized samples as well as the reference samples at the temperature of 473 K. The initial hydrogen pressure during desorption is 0.005 MPa. Although limited amounts of hydrogen can be desorbed at this relatively low temperature, differences in the hydrogen desorption rate between the Ni-containing and Mg@Gn samples illustrate the same catalytic effect of Ni, especially in the $Mg@Ni_8Gn_2$ sample. The positive effect of Ni/Gn additives on the dehydriding rate almost does not change in the case of high temperatures (as shown in Fig. 6). More detailed capacities of hydrogen desorbed for all the samples are listed in Table 1. Results show that in the absence of Ni, Mg@Gn sample desorbs a negligible amount of hydrogen (0.88 wt.%) even at the temperature as high as 543 K, implying that graphene nanoplates alone have a slight beneficial effect on the desorption rate. Adequate combination of transition metal Ni with graphene nanoplates, however, exerts a huge impact on dehydriding behavior. Surprisingly, compared with the others, the $Mg@Ni_8Gn_2$ sample presents the best performance, desorbing 5.73 wt.% of hydrogen in 1800 s at a relatively low temperature of 523 K. A maximum dehydriding capacity of 5.89 wt.% can be achieved in less than 2500 s (not shown). If the temperature increases to 543 K, all the Ni-containing samples reach 90% of their maximum dehydriding capacities in 1000 s, indicating faster hydrogen desorption kinetics is obtained at elevated temperature. It is suggested to be associated with the presence of intermetallic Mg_2Ni, which provides positive effects during the hydriding/dehydriding procedure via a porthole effect combined with microstrain-induced hydrogen sorption mechanism and it will be analyzed in the following section. Note that high Ni content does not always bring about the improvement of dehydriding performance for this current system. As indicated by the reference sample Mg@Ni, which contains the highest Ni amount of 10 wt.%, however, it shows intermediate behavior between the high Ni loading samples (e.g. $Mg@Ni_6Gn_4$ and $Mg@Ni_8Gn_2$) and the low Ni loading samples (e.g. $Mg@Ni_2Gn_8$ and $Mg@Ni_4Gn_6$), independent of

the temperature. The microstructure and phase distribution in the matrix are thought to be responsible for the significant discrepancy of hydriding/dehydriding properties in the Ni-containing samples. It should be noted that despite that the best hydrogen sorption performance at low temperature is achieved for the sample $Mg@Ni_8Gn_2$, the experimental conditions do not mean the optimized one when it comes to the loading amount of Ni or ball milling treatment process.

To facilitate comparison, representative hydrogen sorption data for Mg hydride systems are summarized in Table 2, involving various additional agents and versatile synthetic methods.[17, 19, 35, 36, 40, 41, 50-54] In general, the MgH_2-based composites do not exhibit desirable absorption/desorption kinetics until a relatively high temperature (e.g. 473 K for hydrogen absorption and 543 K for hydrogen desorption) and rigorous pressure (e.g. 3.0 MPa of hydrogen pressure for hydrogen absorption and high vacuum for hydrogen desorption) are set. In addition, although nanometric Mg/MgH_2 composites and the methods of merging custom-made materials show great potential of solving practical storage, only few impressive improvements of the thermodynamic or kinetic properties of hydrogen sorption have been made. The probable reasons may be associated with their relatively lower surface activity. By incorporating Mg hydride with Ni/Gn catalysts, our products display superb kinetics for both hydriding and dehydriding under relatively moderate temperatures, suggesting the ultra-high activity of the HCS+MM products.

Our synthesis of MgH_2-based composites is involved in $Mg@Ni_xGn_{10-x}$ composites preparation (by HCS) in the presence of Ni-containing catalysts and the grain refinement process (by MM) (see Fig. 7). When we use Ni/Gn hybrid catalysts as the additives (Fig. 7a), the in situ formed Mg_2NiH_4 nano particles are more prone to distribute homogenously into/onto the Mg/MgH_2 matrix in the HCS process as a consequence of the fully dispersed starting materials. Afterwards, the high dispersibility of Mg_2NiH_4 phase can be further enhanced by using a short time ball milling, which is supposed to be an effective method to prepare highly active nanosized powders with the uniform distribution of the additional agents. In the case of Fig. 7b, however, using commercial nano Ni powder as the starting material, the dispersive situation for Mg_2NiH_4 is quite different since the Mg_2NiH_4 would easily agglomerate into much larger particles in the absence of restricted material.[55]

As evidenced by TEM images, graphene nanoplates could act as a structural support for loading Ni NPs. Via a space steric effect it leads to a homogenous dispersion of the in situ formed ultrafine Mg_2NiH_4 phase during HCS and MM process, which is essential for the catalyzed hydrogen absorption/desorption of Mg. Besides, due to its unique thermal conductivity and electron mobility, the graphene nanoplates were supposed to provide a thermal and electron-conductive pathway during the H_2 absorption/desorption process.

We also investigated the thermodynamic aspect of the HCS+MM products of Mg hydride in the presence of Ni/Gn additives, and the representative sample of $Mg@Ni_8Gn_2$ was chosen for pressure−composition−isothermal (PCI) measurements. The PCI plots at 533, 573 and 603 K of $Mg@Ni_8Gn_2$ composite are shown in Fig. S5a (see ESI†). Two plateaus are distinguishable in the curves, independent of the temperature and the absorption/desorption reaction. Hydrogen sorption reactions for Mg/MgH_2 and Mg_2Ni/Mg_2NiH_4 should be responsible for the lower plateau and the higher one, respectively, further evidencing the XRD results. It is worthy to note that the plateau for Mg_2Ni/Mg_2NiH_4 seems less well defined and develops a small slope, which might be caused by modifications of MM. A similar phenomenon has been observed in the study of Zaluska.[34] The corresponding van't Hoff plots ($\ln P$ vs. $1/T$) for both hydrogen absorption and desorption of MgH_2 were conducted as shown in Fig. S5b (see ESI†). According to the fitting line from the experimental data, the hydride formation and decomposition reaction enthalpy (ΔH) are calculated to be -74.6 and 78.3 kJ/mol, respectively, being very close to the theoretical values.[56] The results indicate that only minor thermodynamic change can be reached in the $Mg@Ni_8Gn_2$ composite.

To gain further insight into the hydrogen sorption behavior, the activation energy (E_a) was determined in the case of hydrogen desorption for the same sample. In this study, due to the simplicity and reliability,[57] JMA (Johnson-Mehl-Avrami) model (see equation 2) was used for the determination of the dehydriding activation energy in the $Mg@Ni_8Gn_2$ composite.

$$\ln[-\ln(1-\alpha)] = n \ln t + n \ln k \quad (2)$$

Where k is the reaction rate constant, n is the Avrami exponent of reaction order, and α is the fraction transformed at time t. The sample with reacted fraction of $0.1 < \alpha < 0.7$ was used in this study. Fig. 8 shows the JMA plots of $\ln[-\ln(1-\alpha)]$ *vs.* $\ln(t)$ for the dehydrogenation of the $Mg@Ni_8Gn_2$ composite at the temperatures of 523, 553 and 573 K, respectively. By plotting a straight line representing $\ln[-\ln(1-\alpha)]$ *vs*. $\ln(t)$, with the slope n and the intercept $n\ln(k)$, the rate constant k can be obtained for each temperature.

Then the activation energy for hydrogen desorption can be calculated according to the Arrhenius equation:

$$E_a = -RT\ln(k/k_0) \quad (3)$$

Where E_a is the activation energy, k is a time-dependent reaction rate constant, k_0 is the Arrhenius constant, R is the gas constant and T temperature. The value of dehydriding activation energy for the $Mg@Ni_8Gn_2$ composite determined from Fig. 9 is 71.8 kJ/mol, which is much lower than the as-received commercial MgH_2 (160 kJ/mol)[58] and this value is also of high comparability in the related studies. A similar reduction in the value of E_a was observed in our previous work[45] and our current study indicates that prominent enhancement in hydrogen sorption kinetics is achievable even in the absence of precious metal Pd.

The above performances of Mg@Ni/Gn composites as well as the reference samples prepared by HCS+MM imply significant changes in the hydrogen storage properties of Mg hydride. However, PCI measurements showed no essential difference in the thermodynamic property between the $Mg@Ni_8Gn_2$ sample and conventional MgH_2. Alternatively, we

highlight substantial kinetic changes in hydrogen sorption of the HCS+MM products of MgH_2-based composites in the presence of Ni/Gn additives. We suggest it is caused by a combination of high activation surface and highly dispersive ability of in situ formed nanosized Mg_2NiH_4 as a consequence of ball milling treatment. The particular distribution of Mg_2NiH_4 phase, as indicated in TEM examinations, is supposed to play an important role in catalyzing Mg hydride absorption/desorption. The catalytic effect of Mg_2Ni on the hydrogen sorption of Mg hydride has been revealed in many related studies due to its more superior hydrogen sorption properties than MgH_2 in both kinetic and thermodynamic aspects. Here, to support our findings, we assume a mechanism combining porthole effect with mocrostrain-induced sorption exists in this Mg-Mg_2Ni system.

Fig. 10 displays the schematic drawing for the porthole effect of Mg_2Ni in the Mg-Mg_2Ni system. In the Ni-containing samples, in situ generated Mg_2NiH_4 transforms into Mg_2Ni after thermal desorption and it will act as portholes like metal Ti, V, Ni, Pd particles to initially adsorb H_2 and dissociate H_2 into H atoms. There should be at least three steps involved: H_2 diffusion at the composite surface (step 1); H_2 dissociative chemisorption onto Mg_2Ni nanoparticles prior to the Mg matrix (step 2); the migration of H atoms onto/into the Mg matrix (step 3).[39, 47] This will yield a more significant reduction in hydrogenation barrier than in the case of bulk Mg. In addition, in the Mg-Mg_2Ni system, an interaction between close neighbors of Mg and Mg_2Ni might take place via the effect known as expansion-strain-absorption mechanism.[34] It can be explained as follows: based on the porthole effect of Mg_2Ni, H_2 is dissociated into H atoms and captured by the homogenously distributed Mg_2Ni particles; Mg_2Ni absorbs H to form Mg_2Ni hydrides, being accompanied by volume expansion and micro strain; this microstructure change affects the attached Mg neighbor and hence triggers its hydrogen absorption. Once the absorption of Mg is initiated, further hydrogen absorption will proceed through the same mechanism inside the Mg matrix. Note that only marginal Mg_2NiH_4 is required in the composite to cause a sufficient synergetic effect for hydrogen absorption. Furthermore, the dispersion state of the catalytic active sites is crucial to facilitate the catalytic process. That's why the Ni/Gn-containing samples exhibit ultrahigh hydrogen storage performances. The anastrophic mechanism named porthole effect combined with contraction-strain-desorption effect is thought to be applicative in the case of dehydrogenation.

Conclusions

In summary, we have shown the possibility of enhancing dramatically the hydrogen sorption performance at moderate temperatures for Mg hydride system by adding a specific catalyst, namely Ni decorated graphene nanoplates. Microstructural characterization demonstrates that nanometric in situ formed Mg_2NiH_4 particles homogenously distribute into/onto the matrix of the composites. Property measurements of hydrogen sorption of the Ni/Gn-containing composites as well as those of compared samples present clear evidence for their extraordinarily high hydrogen capacity with an impressive fast kinetics in both hydrogenation and dehydrogenation. Particularly, the Mg@Ni_8Gn_2 composite absorbs 6.28 wt.% of hydrogen in 100 s at 373 K and desorbs 5.73 wt.% of hydrogen in 1800 s at 523 K. The activation energy for the dehydrogenation of MgH_2 is 71.8 kJ/mol in the same composite, suggesting a sharp reduction of the barrier to the dehydriding reaction compared with the commercial MgH_2. To our knowledge, the present results of hydrogen sorption kinetics represent competitive data in the related studies under the similar conditions. On the other hand, the hydride formation and decomposition reaction enthalpy (ΔH) for the Mg/MgH_2 are determined as -74.6 and 78.3 kJ/mol, respectively, suggesting no essential thermodynamic change for the Mg@Ni_8Gn_2 composite. We suggest that the highly dispersive ability and the catalytic effect of the in situ formed nanosized Mg_2NiH_4 are responsible for the remarkable enhancement of hydrogen sorption kinetics in the Mg@Ni/Gn composites. We assume a mechanism, in which porthole effect of the locally introduced Mg_2Ni catalytic phase and the microstrain-induced hydrogen sorption effect coexist, functions in this Mg-Mg_2Ni system. Our results demonstrate that graphene-based nano hybrid in the presence of metal NPs can greatly enhance the hydrogen sorption kinetics of the Mg hydride system and offer tremendous potential for the practical application.

Acknowledgements

This work was supported by the National Natural Science Foundation of China (51471087, 51571112), Natural Science Foundation of the Jiangsu Higher Education Institutions of China (13KJA430003), Innovation Foundation for Graduate Students of Jiangsu Province (KYLX_0741), Qing Lan Project and the Priority Academic Program Development (PAPD) of Jiangsu Higher Education Institutions.

References

1 S. Chu, A. and Majumdar, *Nature*, 2012, 488, 294-303.
2 P. Jena, *J. Phys. Chem. Lett.*, 2011, 2, 206-211.
3 J. Graetz, *Chem. Soc. Rev.*, 2009, 38, 73-82.
4 L. Schlapbach and A. Zuttel, *Natur*e, 2001, 414, 353-358.
5 Y.F Liu, K. Zhong, K. Luo, M.X. Gao, H.G. Pan and Q.D. Wang, *J. Am. Chem. Soc.*, 2009,131, 1862-1870.
6 M.B. Ley, L.H. Jepsen, Y.S. Lee, Y.W. Cho, J.M.B. von Colbe, M. Dornheim, M. Rokni, J.O. Jensen, M. Sloth, Y. Filinchuk, J.E. Jorgensen, F. Besenbacher and T.R. Jensen, *Mater. Today*, 2014, 17, 122-128.
7 H. Reardon, J.M. Hanlon, R.W. Hughes, A. Godula-Jopek, T.K. Mandal, and D.H. Gregory, *Energy Environ. Sci.*, 2012, 5, 5951-5979.
8 Y.P. Pang, Y.F. Liu, M.X. Gao, L.Z. Ouyang, J.W. Liu, H. Wang, M. Zhu and H.G. Pan, *Nat. Commun.*, 2014, 5, 3519.
9 K.F. Aguey-Zinsou and J.R. Ares-Fernández, *Energy Environ. Sci.*, 2010, 3, 526-543.
10 I.P. Jain, C. Lal and A. Jain, *Int. J. Hydrogen Energy*, 2010, 35, 5133-5144.

11 P. Chen and M. Zhu, *Mater. Today*, 2008, 11, 36-43.
12 C.J. Chung, C. Nivargi, B. Clemens, *Phys. Chem. Chem. Phys*., 2015, 17, 28977-28984.
13 J. Chen, G.L. Xia, Z.P. Guo, Z.G. Huang, H.K. Liu, X.B. Yu, *J. Mater. Chem. A*, 2015, 3, 15843-15848.
14 Y. Wang, C.H. An, Y.J. Wang, Y.N. Huang, C.C. Chen, L.F. Jiao, H.T. Yuan, *J. Mater. Chem. A*, 2014, 2, 16285-16291.
15 H.Y. Shao, G.B. Xin, J. Zheng, X.G. Li and E. Akiba, *Nano Energy*, 2012, 1, 590-601.
16 M. Dornheim, S. Doppiu, G. Barkhordarian, U. Boesenberg, T. Klassen, O. Gutfleisch and R. Bormann, *Scripta Mater.*, 2007, 56, 841-846.
17 K.J. Jeon, H.R. Moon, A.M. Ruminski, B. Jiang, C. Kisielowski, R. Bardhan and J.J. Urban, *Nat. Mater.*, 2011, 10, 286-290.
18 X.B. Yu, Y.H. Guo, H. Yang, Z. Wu, D.M. Grant and G.S. Walker, *J. Phys. Chem. C*, 2009, 113, 5324-5328.
19 N.S. Norberg, T.S. Arthur, S.J. Fredrick and A.L. Prieto, *J. Am. Chem. Soc.*, 2011, 133, 10679-10681.
20 R.W.P. Wagemans, J.H. van Lenthe, P.E. de Jongh, A.J. van Dillen and K.P. de Jong, *J. Am. Chem. Soc.*, 2005, 127, 16675-16680.
21 W.Y. Li, C.S. Li, H. Ma and J. Chen,*J. Am. Chem. Soc.*, 2007, 129, 6710-6711.
22 J.J. Liang, *Appl. Phys. A*, 2005, 80, 173-178.
23 S. Zhang, A.F. Gross, S.L. Van Atta, M. Lopez, P. Liu, C.C. Ahn, J.J. Vajo and C.M. Jensen, *Nanotechnology*, 2009, 20, 204027.
24 T.K. Nielsen, K. Manickam, M. Hirscher, F. Besenbacher and T.R. Jensen, *ACS Nano*, 2009, 3, 3521-3528.
25 M. Konarova, A. Tanksale, J. Norberto Beltramini and G. Qing Lu, *Nano Energy*, 2013, 2, 98-104.
26 C. Zlotea, F. Cuevas, J. Andrieux, C. Matei Ghimbeu, E. Leroy, E. Léonel, S. Sengmany, C. Vix-Guterl, R. Gadiou, T. Martens and M. Latroche, *Nano Energy*, 2013, 2, 12-20.
27 P.E. de Jongh, R.W.P. Wagemans, T.M. Eggenhuisen, B.S. Dauvillier, P.B. Radstake, J.D. Meeldijk, J.W. Geus and K.P. de Jong, *Chem. Mater.*, 2007, 19, 6052-6057.
28 G.L. Xia, Y.B. Tan, X.W. Chen, D.L. Sun, Z.P. Guo, H.K. Liu, L.Z. Ouyang, M. Zhu and X.B. Yu, *Adv. Mater.*, 2015, 27, 5981-5988.
29 C. Zlotea, Y. Oumellal, S.J. Hwang, C.M. Ghimbeu, P.E. de Jongh, M. Latroche, *J. Phys. Chem. C*, 2015, 119, 18091-18098.
30 M.H. Braga and A. El-Azab, *Phys. Chem. Chem. Phys.*, 2014, 16, 23012-23025.
31 W. Liu, E.J. Setijadi and K.F. Aguey-Zinsou, *J. Phys. Chem. C*, 2014, 118, 27781-27792.
32 B. René, A. Philipp, H.M. Johannes, P.d.J. Krijn and E.d.J. Petra, *Nanotechnology*, 2009, 20, 204019.
33 X.Z. Xiao, C.C. Xu, J. Shao, L.T. Zhang, T. Qin, S.Q. Li, H.W. Ge, Q.D. Wang, L.X. Chen, *J. Mater. Chem. A*, 2015, 3, 5517-5524.
34 A. Zaluska, L. Zaluski and J.O. Ström-Olsen, *J. Alloy. Compd.*, 1999, 289, 197-206.
35 J. Cui, J.W. Liu, H. Wang, L.Z. Ouyang, D.L. Sun, M. Zhu and X.D. Yao, *J. Mater. Chem. A*, 2014, 2, 9645-9655.
36 A.M. Ruminski, R. Bardhan, A. Brand, S. Aloni and J.J. Urban, *Energy Environ. Sci.*, 2013, 6, 3267-3271.
37 J. Lu, Y.J. Choi, Z.Z. Fang, H.Y. Sohn and E. Rönnebro, *J. Am. Chem. Soc.*, 2010, 132, 6616-6617.
38 H.J. Lin, J.J. Tang, Q. Yu, H. Wang, L.Z. Ouyang, Y.J. Zhao, J.W. Liu, W.H. Wang and M. Zhu, *Nano Energy*, 2014, 9, 80-87.
39 W. Xie, D.J. West, Y. Sun and S. Zhang, *Nano Energy*, 2013, 2, 742-748.
40 T. Liu, C.G. Chen, F. Wang and X.G. Li, *J. Power Sources*, 2014, 267, 69-77.
41 L.T. Zhang, X.Z. Xiao, C.C. Xu, J.G. Zheng, X.L. Fan, J. Shao,Q. S. Li, H.W. Ge, Q.D. Wang and L.X. Chen, *J. Phys. Chem. C*, 2015, 8554-8562.
42 F. Karimi, P. Klaus Pranzas, C. Pistidda, J.A. Puszkiel, C. Milanese, U. Vainio, M. Paskevicius, T. Emmler, A. Santoru, R. Utke, M. Tolkiehn, C.B. Minella, A.-L. Chaudhary, S. Boerries, C.E. Buckley, S. Enzo, A. Schreyer, T. Klassen, M. Dornheim, *Phys. Chem. Chem. Phys*., 2015, 17, 27328-27342.
43 G.. Li, H. Kobayashi, J.M. Taylor, R. Ikeda, Y. Kubota, K. Kato, M. Takata, T. Yamamoto, S. Toh, S. Matsumura and H. Kitagawa, *Nat. Mater.*, 2014, 13, 802-806.
44 Y. Wang, L. Li, C.H. An, Y.J. Wang, C.C. Chen, L.F. Jiao and H.T. Yuan, *Nanoscale*, 2014, 6, 6684-6691.
45 J.G. Yuan, Y.F. Zhu and L.Q. Li, *Chem. Commun.*, 2014, 50, 6641-6644.
46 S. Navalon, A. Dhakshinamoorthy, M. Alvaro and H. Garcia, *Chem. Rev.*, 2014, 114, 6179-6212.
47 M. Lototskyy, J.M. Sibanyoni, R.V. Denys, M. Williams, B.G. Pollet and V.A. Yartys, *Carbon* , 2013, 57, 146-160.
48 S.D. House, J.J. Vajo, C. Ren, A.A. Rockett and I.M. Robertson, *Acta Mater.*, 2015, 86, 55-68.
49 P. Adelhelm and P.E. de Jongh, *J. Mater. Chem.*, 2011, 21, 2417-2427.
50 M.G. Verón, H. Troiani and F.C. Gennari, *Carbon*, 2011, 49, 2413-2423.
51 C. Zhou, Z.Z. Fang, C. Ren, J. Li and J. Lu, *J. Phys. Chem. C*, 2013, 117, 12973-12980.
52 G. Liu, Y.J. Wang, C. Xu, F.Y. Qiu, C.H. An, L. Li, L.F. Jiao and H.T. Yuan, *Nanoscale*, 2013, 5, 1074-1081.
53 B.H. Chen, C.H. Kuo, J.R. Ku, P.S. Yan, C.J. Huang, M.S. Jeng and F.H. Tsau, *J. Alloy. Compd.*, 2013, 568, 78-83.
54 Y.N. Liu, J.X. Zou, X.Q. Zeng, X.M. Wu, D.J. Li and W.J. Ding, *J. Phys. Chem. C*, 2014, 118, 18401-18411.
55 Y.F. Zhu, Z.B. Liu, Y. Yang, H. Gu, L.Q. Li and M. Cai, *Int. J. Hydrogen Energy*, 2010, 35, 6350-6355.
56 M. Paskevicius, D.A. Sheppard and C.E. Buckley, *J. Am. Chem. Soc.*, 2010, 132, 5077-5083.
57 C.Y. Zhu and T. Akiyama, *Cryst. Growth. Des.*, 2012, 12, 4043-4052.
58 W.P. Cai, X.S. Zhou, L.D. Xia, K.L. Jiang, S.M. Peng, X.G. Long, J.H. Liang, *J. Mater. Chem. A*, 2014, 2, 16369-16372.

Graphical abstract

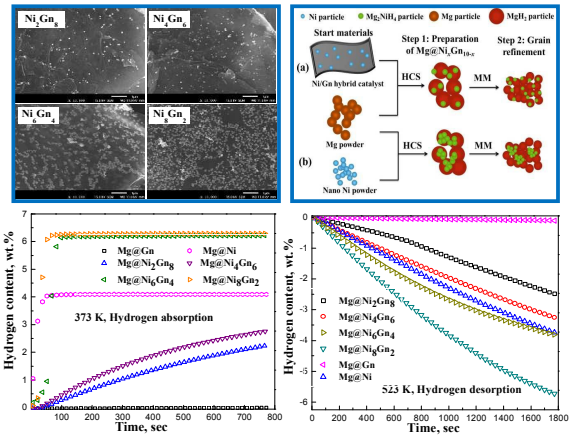

Ni/Gn catalysts were introduced to obtain Mg-based composites via HCS+MM for excellent H_2 sorption properties at moderate temperatures.

Table 1 Hydrogen absorption/desorption capacities at different temperatures of $Mg@Ni_xGn_{10-x}$ (x =2, 4, 6, 8) as well as the reference samples Mg@Ni and Mg@Gn composites prepared by HCS+MM[a].

T (K)	Hydrogen absorption/desorption capacities (wt. %)					
	$Mg@Ni_2Gn_8$	$Mg@Ni_4Gn_6$	$Mg@Ni_6Gn_4$	$Mg@Ni_8Gn_2$	Mg@Ni	Mg@Gn
373	2.23 / - -	2.75 / - -	6.21 / - -	6.28 / - -	4.06 / - -	0.02/ - -
393	3.68 / - -	3.91 / - -	6.61 / - -	6.32 / - -	4.67 / - -	0.03/ - -
473	5.99 / 0.38	5.98 / 0.63	6.64/ 0.76	6.60 / 1.48	5.12/0.48	4.33/ 0.03
523	6.05 / 2.48	6.07 / 3.25	6.67/ 3.81	6.66 / 5.73	5.39/ 3.70	5.21/ 0.11
543	6.04 / 5.50	6.19 / 5.69	6.74/ 6.00	6.51 / 5.90	5.77/ 4.56	5.69/ 0.88

[a] The values of hydrogen absorption and desorption capacities for all the samples are collected in 100 s and 1800 s, respectively.

Table 2 Summary of hydrogen absorption/desorption data for MgH_2 system available in the literature

Reference	Method	System component	Hydrogen absorption	Hydrogen desorption
[17]	Solution reducing	MgH_2@5wt.%PMMA	3.5 MPa, 200℃, 5.97 wt.% for Mg (4.0 wt.% total) /30 min	0 MPa, 200℃, 4 wt.% total/4 h
[50]	Ball milling	MgH_2@5wt.%Co +5wt.%MWCNTs	2.0 MPa, 250℃, 6.5 wt.%/100 s	0.02 MPa, 250℃, 6.5 wt.%/85 min; 275℃, 6.5 wt.%/1400 s
[51]	Ball milling	MgH_2@5 at.% $TiMn_2$	0.1 MPa, 25℃, 3.3 wt.%/4 h	—
[40]	Hydrogen plasma-metal reaction	Mg@9.2wt.%$TiH_{1.97}$ +3.7wt.%$TiH_{1.5}$	4 MPa, 25℃, 4.3 wt.%/10 min; 100℃, 4.6 wt.%/5 min	0.001 MPa, 300℃, 3.5 wt.%/5 min
[52]	Ball milling	MgH_2@5 wt% GNS	2 MPa, 150℃, 6.0 wt.%/180 min; 200℃, 6.3 wt.%/40 min	0.005 MPa, 300℃, 6.1 wt.%/40 min
[53]	Ball milling	Mg@30 wt.%FeTi +1 wt.%CNTs	2 MPa, 150℃,6.6 wt.%/60 s	—
[21]	Vapor-transport	Mg nanowires	2 MPa, 100℃, 2.93 wt.%/30min;	0.02 MPa, 200℃, 3.28 wt.%/30 min
[54]	Solution copreciptation	Mg@10 wt.%Ni	3 MPa, 125℃, 4.93 wt.%/45 s, 5.8 wt.%/2h	—
[35]	Ball milling and solution reducing	Mg@TM(TM: Ti, Nb, V, Co, Mo, or Ni)	2 MPa, 250℃, 6.0 wt.%/5 min (for Mg@Ni)	0.001 MPa, 250℃, 2.0 wt.%/10 min; 275℃, 3.6 wt.%/10 min (for Mg@Ni)
[19]	Solution reducing	Mg nanoparticles	1.15~0.9 MPa, 300℃, 5.7 wt.%/60 s	0.06~0.02 MPa, 335℃, 4.8 wt.%/1500 s
[36]	Solution reducing	Mg@35 wt.%PMMA	3 MPa, 200℃, 6.95 wt.% Mg (4.6 wt.% total) /2 h	—
[41]	Ball milling	Mg@5 wt.%NbH_x	2.2 MPa, 100℃, 3.7 wt.%/60 s	0.003 MPa, 300℃, 7.0 wt.%/9 min; 270℃, 4.3 wt.%/5 min
This study	**HCS+MM**	**MgH_2@ 10 wt.% (Gn+Ni)**	**3 MPa, 100℃, 6.28 wt.% /100 s**	**0.005 MPa, 250℃, 5.73 wt.%/1800 s**

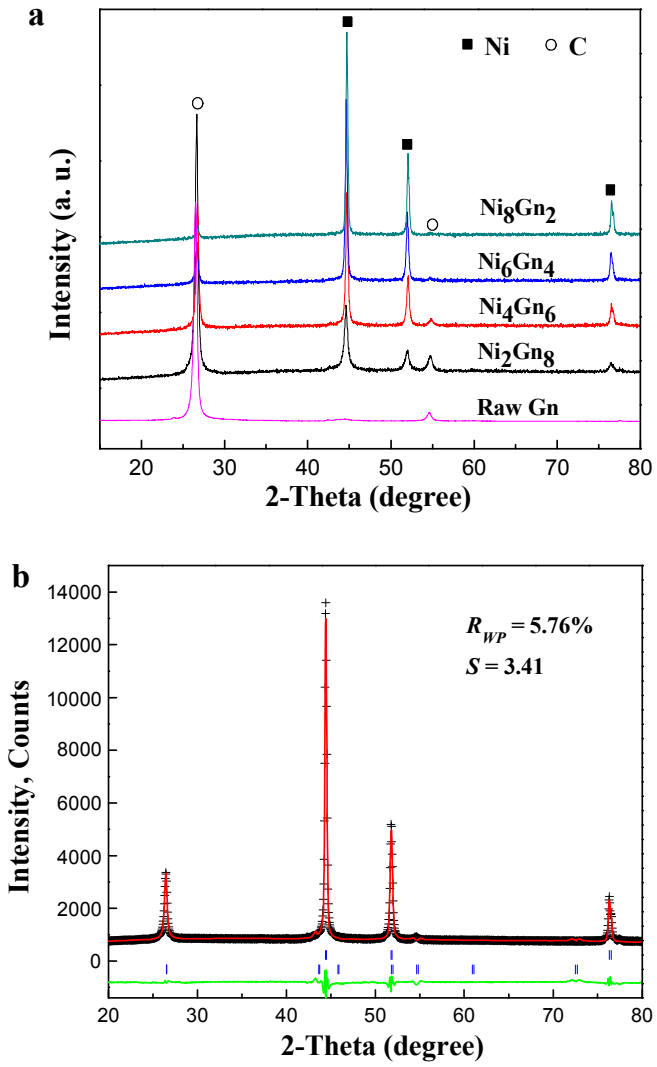

Fig. 1 (a) X-ray diffraction patterns of as-synthesized Ni_xGn_{10-x} (x=2, 4, 6, 8) nano hybrid catalysts and the raw graphene nanoplates; (b) The Rietveld analysis results of the Ni_6Gn_4 catalyst, position of Bragg peaks of constituent phases are shown (from top to bottom): Ni 61.1 wt.%, C 38.9 wt.%.

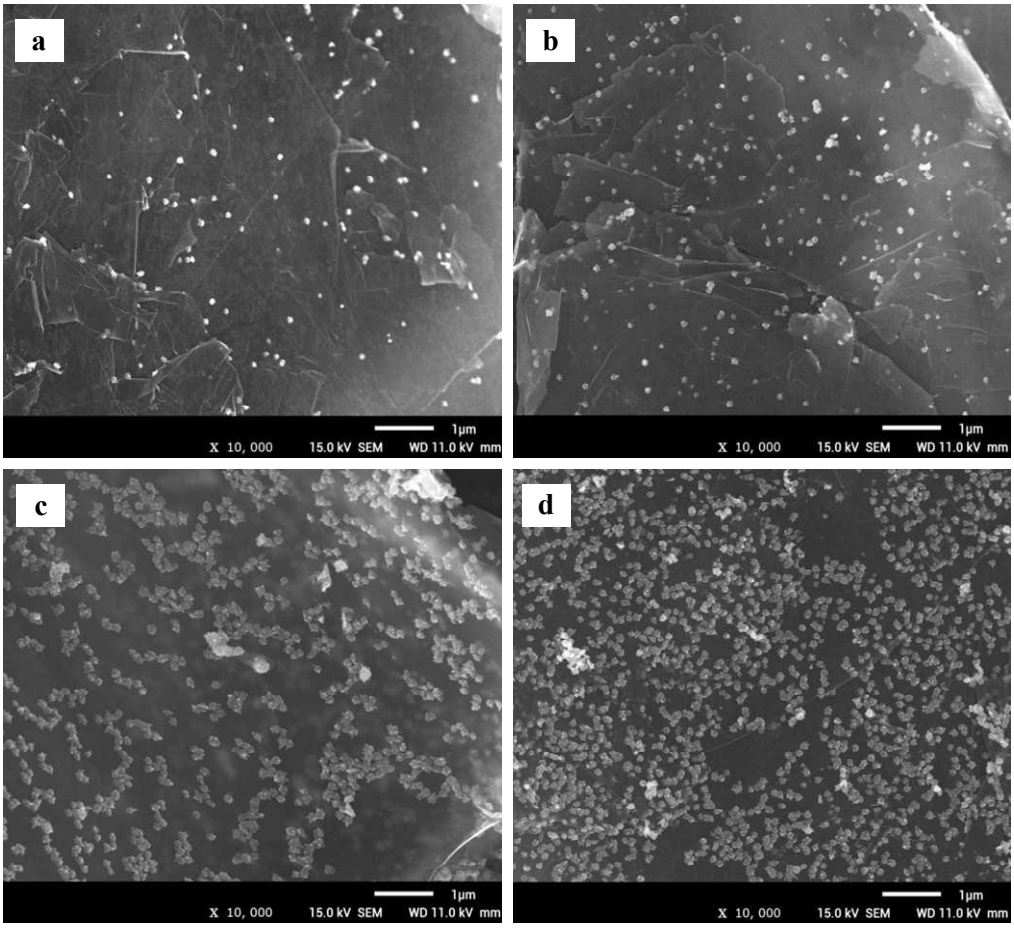

Fig. 2 SEM images of as-synthesized Ni_xGn_{10-x} (x=2, 4, 6, 8) nano hybrid catalysts. (a) Ni_2Gn_8, (b) Ni_4Gn_6, (c) Ni_6Gn_4 and (d) Ni_8Gn_2.

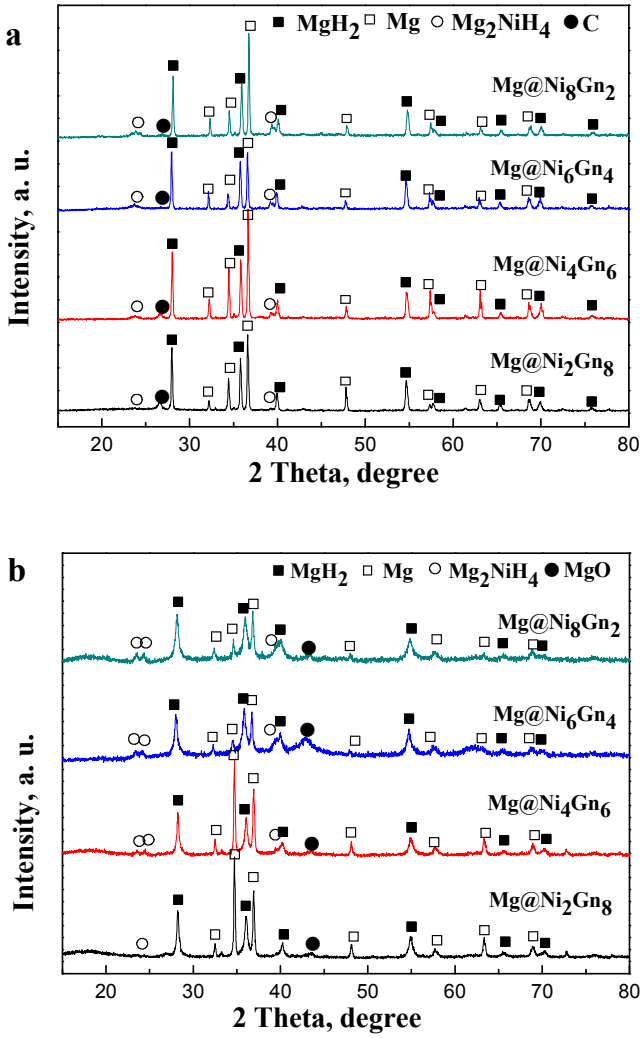

Fig. 3 X-ray diffraction patterns of the Mg@Ni_xGn_{10-x} (x =2, 4, 6, 8) composites prepared by (a) HCS and (b) HCS+MM.

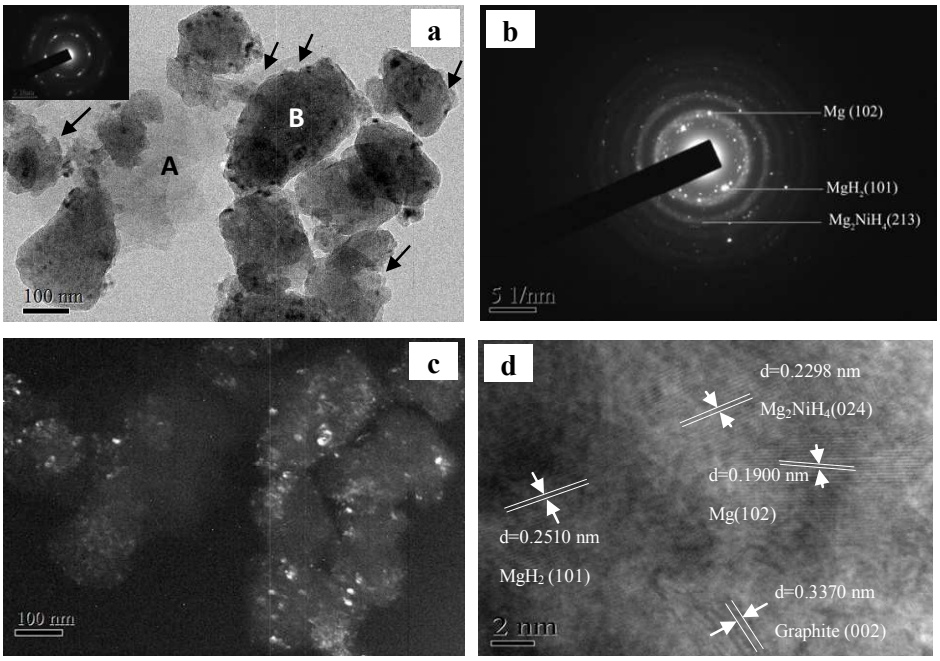

Fig. 4 TEM micrographs of the HCS+MM product of $Mg@Ni_8Gn_2$ sample. (a) Bright-field image, inset-the SAED pattern of corresponding region A confirms the existence of graphene nanoplates (arrows in the image point to the graphene nanoplates); (b) The SAED pattern of region B from the same aggregates of (a); (c) Dark-field image formed with the objective aperture placed over a portion of the Mg_2NiH_4 (213) diffraction ring; (d) A typical HRTEM image.

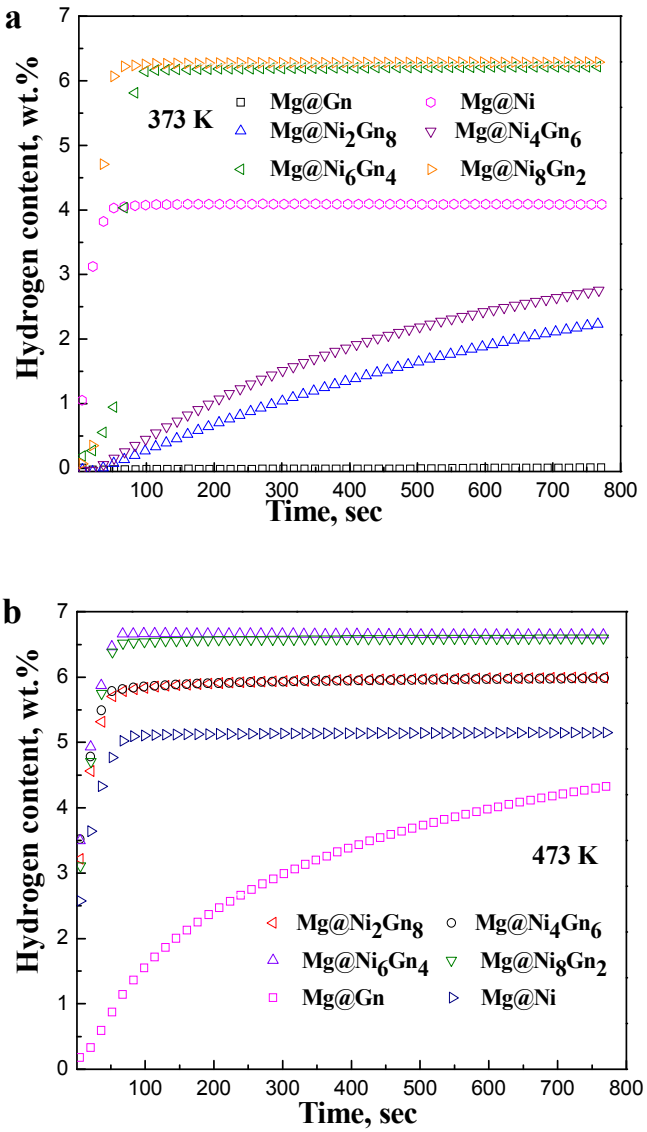

Fig. 5 Hydrogen absorption curves for $Mg@Ni_xGn_{10-x}$(x =2, 4, 6, 8) as well as the reference samples Mg@Ni and Mg@Gn composites prepared by HCS+MM. (a) 373 K; (b) 473 K. The initial hydrogen pressure during absorption is 3.0 MPa.

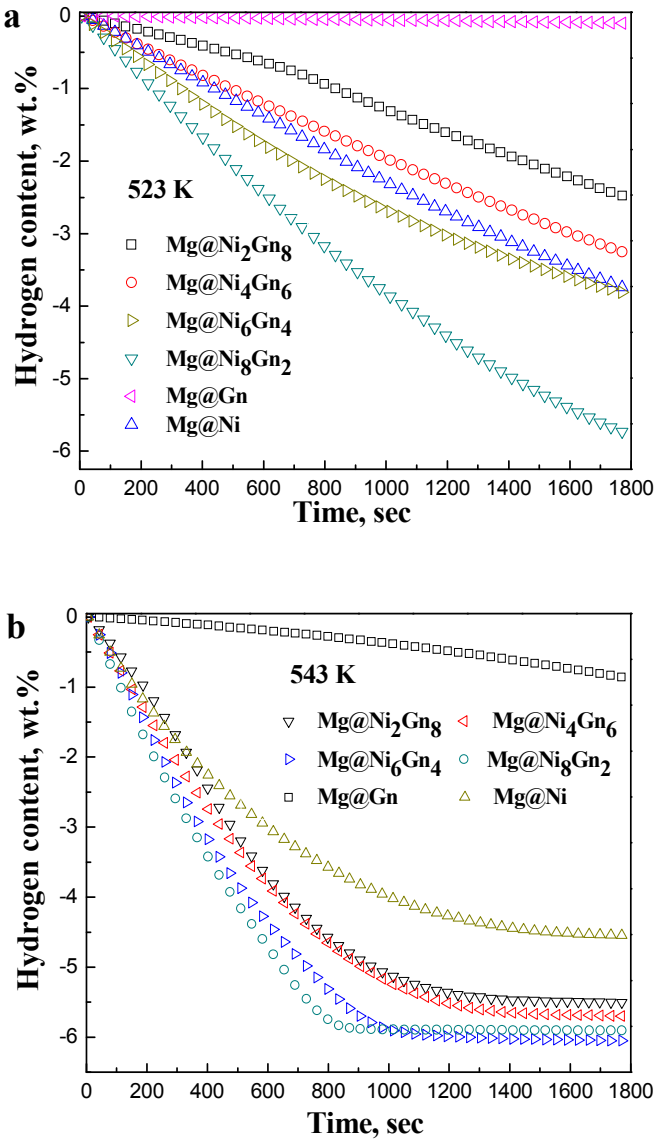

Fig. 6 Hydrogen desorption curves for Mg@Ni$_x$Gn$_{10-x}$ (x =2, 4, 6, 8) as well as the reference samples Mg@Ni and Mg@Gn composites prepared by HCS+MM. (a) 523 K; (b) 543 K. The initial hydrogen pressure during desorption is 0.005 MPa.

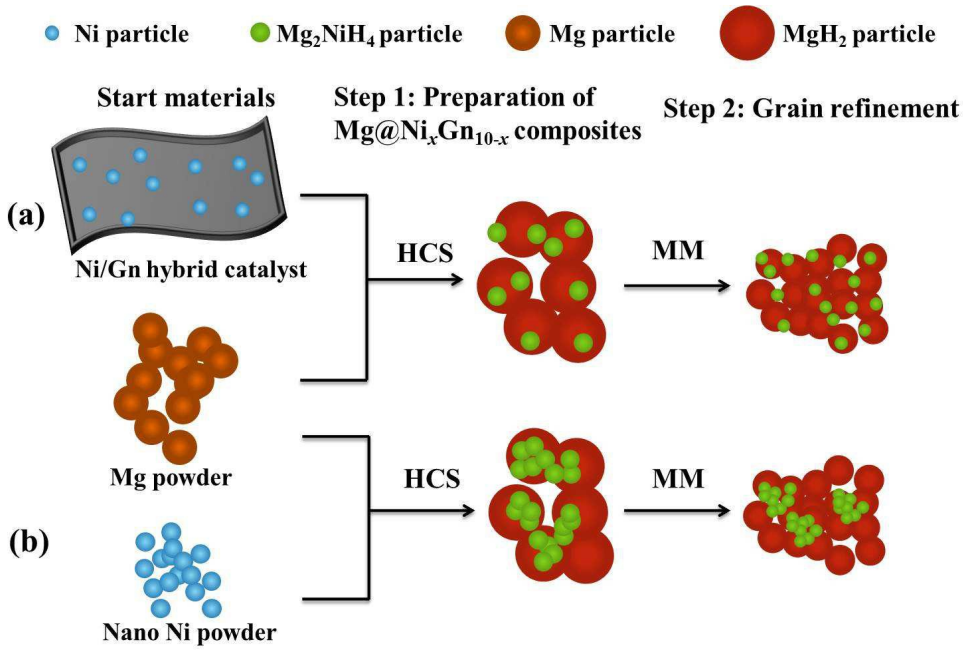

Fig. 7 Schematic illustration for the synthesis (HCS+MM) of $Mg@Ni_xGn_{10-x}$ composites using different additives as the starting material: (a) as-synthesized Ni/Gn hybrid catalyst; (b) as-received nano Ni powder.

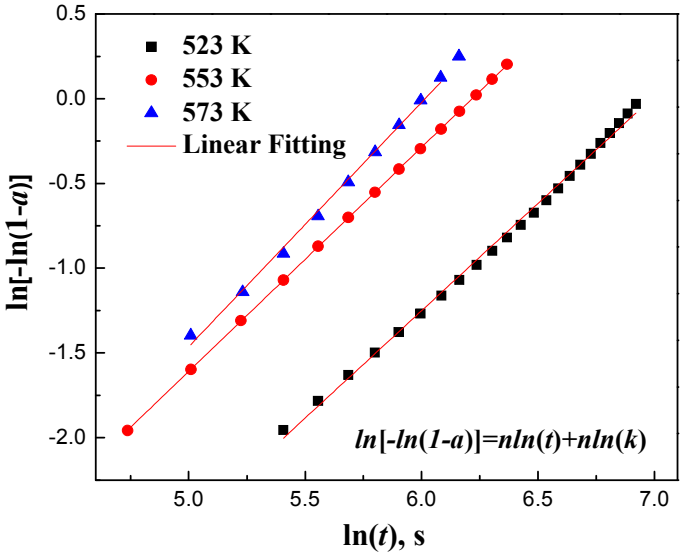

Fig. 8 JMA plots of $\ln[-\ln(1-\alpha)]$ *vs*. $\ln(t)$ for the dehydrogenation of the $Mg@Ni_8Gn_2$ composites at 523, 553 and 573 K, respectively. The sample with reacted fraction of $0.1 < \alpha < 0.7$ was used.

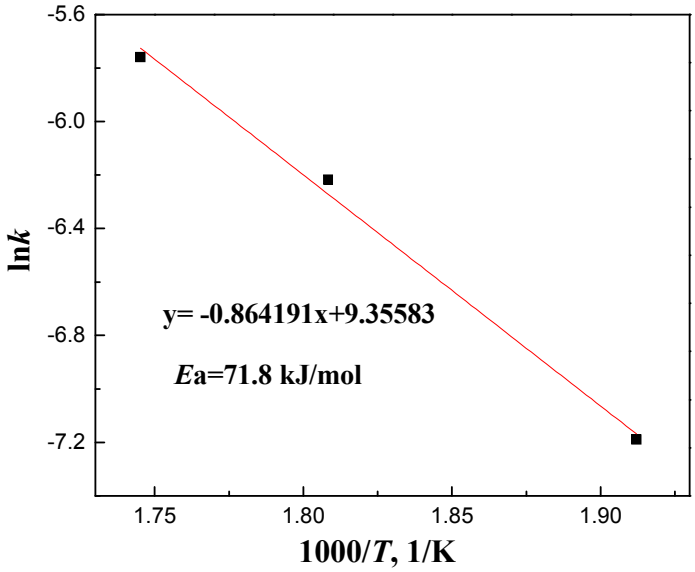

Fig. 9 Arrhenius plots for the dehydriding kinetics of the $Mg@Ni_8Gn_2$ composite.

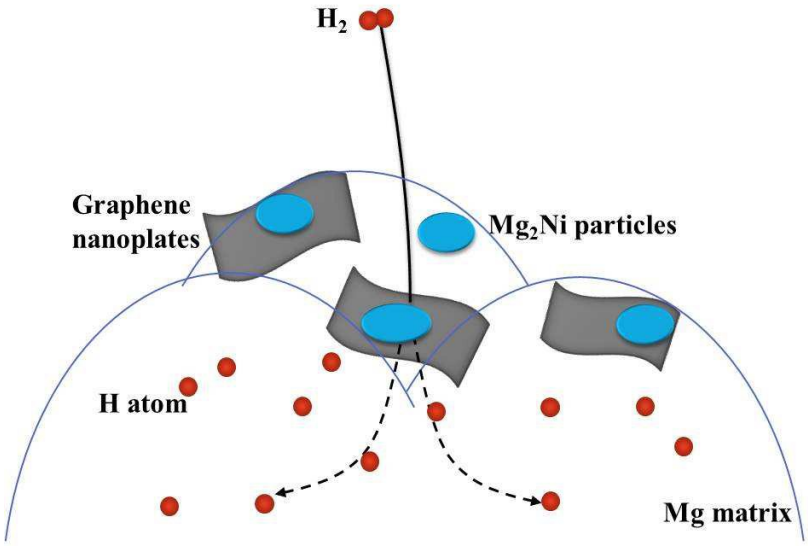

Fig. 10 Schematic drawing for the porthole effect of Mg_2Ni in the $Mg@Ni_xGn_{10-x}$ system. It typically includes 3 steps: (step 1) H_2 diffusion at the surface of the composite; (step 2) H_2 dissociative chemisorption onto Mg_2Ni nanoparticles prior to the Mg matrix followed by (step 3) the migration of H atoms onto/into the Mg matrix.